(Publicado en J. Catalysis 108 (1987) 334-345 (doi: 10.1016/0021-9517(87)90182-5)

Migration of molybdenum into crystalline cavities in molybdate-impregnated NaY zeolite

J.L.G. Fierro, J.C. Conesa, A. López Agudo

Instituto de Catálisis y Petroleoquímica, C.S.I.C., Serrano 119, 28006 Madrid, Spain

Molybdenum-containing Y-type zeolites have been prepared by thermal decomposition of molybdate-impregnated samples according to a nonconventional procedure which uses a constant rate decomposition at very low water vapor pressure (10 N m^{-2}). The combined results of X-ray diffraction, mid-infrared, surface area, and sorption (water and n-hexane) capacity measurements show that zeolite structure was largely retained when the impregnated material was activated at temperatures below 623 K. However, a progressive loss of crystallinity and a parallel decrease of the surface Mo/Si ratio, as obtained from the X-ray photoelectron spectra, was observed at higher temperatures. Furthermore, on heating at higher temperatures (793 K), the electron spin resonance spectra indicated that a fraction of the Mo(V) ions are essentially isolated in the sodalite cages or hexagonal prisms of the zeolite. A mechanism which involves "vaporization" of MoO_3 from the external surface of the zeolite by water vapor is proposed to describe the redistribution of molybdenum in the impregnated precursor.

INTRODUCTION

Molybdenum- (or tungsten-) based hydrotreating catalysts constitute one of the remarkable groups of catalysts that have been so successfully employed in the petroleum industry. As the world's supply of crude oil shifts to heavier sources with substantial sulfur, nitrogen, and heavy metal content, the challenge of removing these catalyst poisons is requiring an imaginative effort to improve molybdenum based catalysts. The exceptional properties of zeolites, including catalytic activity and great resistance to poison by sulfur- and nitrogen-containing organic compounds, provide an incentive to prepare and examine the properties of molybdenum-loaded zeolites. The preparation of these catalysts is difficult since the incorporation of Mo into the porous structure of the zeolite is partially restricted. Several methods, including aqueous ion exchange of the cationic $Mo_2(en)_4^{4+}$ (1) and MoO_2^{2+} complexes, solid-state ion exchange of $MoCl_5$ (1, 3), vapor-phase adsorption of $MoCl_5$ (4) and the neutral $Mo(CO)_6$ complex (5, 6), direct incorporation into the zeolite lattice during zeolite synthesis (7), and conventional impregnation with aqueous solutions of ammonium heptamolybdate (AHM) (8-16) have been used to incorporate Mo in zeolites. In this latter case, the impregnation method results mostly in surface loading, since the oxoanionic or neutral complexes will not penetrate into the zeolite pores

in the presence of water. In principle, this disadvantage can be easily overcome by Mo vaporization from the surface of zeolite crystals and further solid-state exchange of the $MoO_2(OH)_2$ within the pores of the zeolite. This idea, which does not substantially differ from the method first described by Dai and Lunsford (3) for the preparation of Mo-HY and then by Johns and Howe (4) for Mo-H mordenite using the vapor-phase adsorption of $MoCl_5$, has been exploited in this work for the successful preparation of molybdenum-loaded NaY zeolite. Molybdenum migration is expected to occur since during thermal treatment at low residual pressure (10 N m^{-2}) a Mo concentration gradient is generated between the surface and the pores of zeolite. Hence $MoO_2(OH)_2$ diffuses within the zeolite cages. The method, which requires a constant and very low decomposition of the Mo-NaY impregnate, therefore needs long periods of time to attain the highest temperature. Under such conditions, the loss of zeolite crystallinity was significantly smaller than that found on conventionally air-calcined samples. X-ray photoelectron spectroscopy and electron spin resonance have been used to follow the M_O location in the Mo-impregnated NaY zeolite subjected to vacuum decomposition at high temperatures. It is shown that $MoO_2(OH)_2$ vapor diffuses at temperatures above 700 K from the external surface to the zeolite cavities.

EXPERIMENTAL

Sample Preparation

Molybdenum-NaY zeolite samples were prepared by impregnation of NaY zeolite (LZ-Y52 Union Carbide) with an aqueous solution of ammonium heptamolybdate (AHM) of the appropriate concentration to obtain an MoO_3 loading of 10 wt%. The volume of solution was that necessary to completely wet the zeolite carrier, and the pH of the slurry was about 5.4. The excess of water was evaporated till dryness at 343 K in a rotary evaporator. The precursor was subsequently decomposed according to a nonconventional procedure which depends on its controlled dehydration (see below). Aliquots of the sample were withdrawn from the reactor where the decomposition was carried out at temperatures increasing slowly up to 383, 623, 713, and 793 K. These samples will be referred to thereafter as MoT where T indicates the decomposition temperature. In a few of these samples the Mo was partially extracted by solubilization by treating a 1.0-g sample with 100 ml of diluted ammonia solution (3% v/v) for 24 h. The solubilized Mo was determined in the filtrate by atomic absorption spectrometry. The extracted samples so obtained will be referred to as MoTE. As a reference, a 10 wt% Mo-NaY sample was prepared following the same impregnation procedure, but was dried at 383 K overnight, and then calcined at 793 K for 4 h in air. This last sample will be referred as MoA.

Methods

The constant rate decomposition (CRD) procedure was carried out under quasi-isothermal conditions while a constant low pressure (10 N m^{-2}) was maintained in the reactor containing the sample. The reactor temperature was differentially increased by a furnace that was synchronized with duplicate Pirani gauges placed just before and after a capillary leak. Thus, the pumping rate was controlled by the Knudsen flow through the capillary, and the extent of sample decomposition could be calculated at any time. This method needs for its

completion very long periods of time (up to 4 weeks for the Mo 793 sample) since the heating must be very slow in order to avoid buildup of an excessive water vapor pressure. For details, see Ref. (17).

Specific surface areas of the samples were obtained by the monolayer point method nitrogen adsorption isotherm at 77 K, and 0.162 nm^2 was taken as the value of the cross-sectional area of N_2 at this temperature. Adsorption capacities of the preparations were measured with a vacuum microbalance. Polar (H_2O) and nonpolar (n-hexane, Carlo-Erba) adsorbates were used. All samples were thoroughly outgassed at 623 K and were contacted with these adsorbates at 295 K at relative pressures (P/P_0) between 0 and 1. Powder diffraction patterns were obtained under constant instrumental conditions on a Philips PW 1010 diffractometer using nickel-filtered copper Kα radiation.

All X-ray photoelectron spectra (XPS) were recorded on a Vacuum Generators ESCA 3 spectrometer equipped with a magnesium anode (Mg Kα=1253.6 eV) operated at 14 kV and 20 mA. The residual pressure inside the analysis chamber was below 8 x 10^{-7} N m^{-2}. The powdered samples were pressed into small Inox holders (~1 mm height) and then mounted on a long rod which allowed fast entry in the analysis chamber. C 1s, O 1s, Si 2p, Al 2p, Na 1s, and Mo 3d photoemissions were recorded for each sample. The binding energies (BE) were calculated by taking the energy of the 1s photoelectron of carbon contamination as an internal standard at 285.0 eV relative to the Fermi level. The estimated error in BEs is ±0.2 eV.

Electron spin resonance (ESR) spectra were obtained with a Bruker ER 200D spectrometer, operating in the X-band. The spectra were recorded at either 295 or 77 K. A Mn:MgO standard (g_e=2.0066) was used to calibrate the magnetic field. Samples of about 0.050 g placed inside a quartz-probe cell were first outgassed at selected temperatures and, when required, were subsequently contacted with O_2, H_2, or C_3H_6 at pressures of 0.7-7 kN m^{-2}, prior to the recording of their spectra.

Infrared spectra (IR) were recorded in a Perkin-Elmer 580B spectrophotometer interfaced to a data station. The 1400-400 cm^{-1} wavenumber region of the spectrum only was considered. For this purpose, self-supporting wafers of similar thickness and density of ca. 0.030 g cm^{-2} were prepared by pressing an identical amount of powdered samples diluted with KBr in the proportion 1:100.

RESULTS

X-Ray Diffraction

Figure 1 shows X-ray diffraction (XRD) powder patterns of MoT (T=383, 623, 713, and 793 K) preparations. For comparative purposes, the XRD pattern of the NaY parent zeolite, together with that of the MoA sample, are also included in the same figure. The patterns of MoT preparations were similar to that of the NaY zeolite except for the peak intensities. The peak intensities in the MoT series decreased slightly after impregnation with AHM and more markedly with increasing T. The average changes in crystallinity of the MoT samples with reference to the intensity of three most intense peaks at 0.285, 0.371, and 0.571 nm of a 10 wt% MoO_3-

NaY physical mixture were calculated and plotted against T (Fig. 8). Relative crystallinity decreased with increasing T, although this decrease was much less marked than that found in the MoA sample calcined in air by a conventional procedure.

Mid-infrared Spectra

Preliminary data obtained by this technique, reported previously in Ref. (13) and summarized in Fig. 2, give information about the vibrational modes of the zeolite framework in the MoT series, parent NaY, and MoA preparations. All Mo-loaded zeolites showed bands of varying intensity and width, depending on T or on calcination procedure, at about 1140, 1000, 900-920 (shoulder), 800, 705, 585, and 465 cm^{-1}, which are typical for NaY (18, 19). The bands at about 1000, 705, and 465 cm^{-1} are due to internal vibrations of the $(Si,Al)O_4$ tetrahedra of NaY, whereas the bands at about 1140, 800, and 585 cm^{-1} are due to vibrations related to external linkages between tetrahedra and hence sensitive to framework structure. The intensity of the framework vibration bands of the Mo383 and Mo623 samples decreased only slightly as compared with those of the NaY, but calcination at higher temperature (Mo713 and Mo793) resulted in a gradual intensity loss and some band broadening. Comparison between Mo793 and MoA preparations (spectra e and f) showed that the former exhibited more intense bands than the latter. Furthermore, a shoulder (or small band) at about 900-920 cm^{-1}, which was better resolved in the MoA sample, gradually appeared with increasing T. Since this band was absent in the parent NaY zeolite, it is reasonable to associate it with some Mo-O bond vibration, such as Mo=O bonds of a monomeric MoO_4^{2-} species (3, 9) attached to the zeolite framework. The position of the bands did not change in general with T, except for the Mo793 preparation (spectrum e), in which several bands (1000, 800, and 585 cm^{-1}) were shifted slightly toward higher wavenumbers. These shifts, which in turn are accompanied by a marked decrease in band intensities, are also indicative of a loss of zeolite crystallinity.

Adsorption Capacity

The adsorption capacities of n-hexane (nonpolar) and water (polar) were obtained for all MoT preparations from the adsorption isotherms of both adsorbates at 297 K. Figure 3 shows two sets of these isotherms in the entire range of relative pressures for the Mo793 and the parent NaY zeolite samples, indicating always a lower adsorption capacity for n-hexane than for water. The n-hexane isotherm is type I behavior while the water isotherm is a combination of types I and II, with an important increase of the adsorbed amount at P/P_0, above 0.8. In parallel to these measurements, the N_2 adsorption isotherms at 77 K were obtained, and the surface areas were calculated from the apparent monolayer point. These isotherms could not be fitted to the usual two parameter BET equation, showing instead type I behavior. The relative adsorption capacities of both adsorbates (at $P/P_0 = 0.4$) and surface areas of the MoT samples with respect to the parent NaY zeolites (Fig. 8) decreased also with increasing T, in parallel with crystallinity as determined by XRD.

X-Ray Photoelectron Spectra

In order to study the changes in surface composition of the Mo-loaded zeolites, XP spectra of the MoT (T = 383, 623, 713, and 793 K), MoTE (T = 623, and 793 K), and MoA samples were recorded. The BEs found for

all the catalyst constituents agreed with the values expected for a fully oxidized catalyst; no significant differences were detected between the different samples. Changes in the FWHM (full width at half maxima) did occur in the Mo 3d peaks upon increasing temperature of the CRD procedure, as seen in Fig. 4. Mo^{6+} ions, which give characteristic spin-orbit 3d doublets at about 232.8 and 235.8 eV like those present in MoO_3 and $Al_2(MoO_4)_3$ (see, e.g., (20-22)), showed a steady increase in FWHM with increasing T. Another important fact to take into account is the marked difference between the FWHMs of the Mo793 and MoA samples. Although both preparations were calcined at 793 K, the former was conducted under vacuum, according to the CRD procedure, whereas the latter was conducted in air by a conventional calcination. Additionally, the FWHMs of Mo 3d levels in the MoTE samples increased significantly, especially in the Mo793E sample, with respect to those of the unextracted partners.

The most relevant feature of the XP spectra was the change of the photoemission intensities with pretreatments. In an attempt to rationalize these differences, the surface Mo/Si and Mo/(Si + Al) atomic ratios were calculated from the integrated intensities of the peaks. Silicon was taken as basis of calculations since it is, with the exception of O, the most abundant element at the zeolite surface. The equation used was

$$(Mo/Si)_s = (I_{Mo}/S_{Mo})(I_{Si}/S_{Si}) \qquad (1)$$

where S_{Si} and S_{Mo} are the sensitivity factors of Si and Mo, respectively, and I_{Si} and I_{Mo}, the peak intensities of Si 2p and Mo 3d levels, respectively. S factors were taken from Wagner *et al.* (23). The atomic ratios so calculated and those obtained by chemical analysis are summarized in Table 1. It can be seen that the (Mo/Si) ratio changes drastically with pretreatments. In the MoT series this ratio first increased as increasing T, reaching a maximum at about 623 K, and then decreased rapidly. The (Mo/Si), ratio in the Mo793 sample (0.041) is lower than that (0.063) found in the MoA sample, which, in turn, is less than one half of that (0.100) given by chemical analysis. These changes are reported in Fig. 5. The drastic decay of the (Mo/Si) ratio in the Mo623E sample indicates that an important Mo surface concentration was removed from the Mo623E sample during ammonia extraction. However, the Mo removal became less marked in the Mo793 sample.

Electron Spin Resonance

ESR spectra were taken first for samples Mo623 and Mo793. For both of them the spectra showed in some cases a sextet of sharp, equally spaced lines which could be unambiguously assigned to a Mn^{+2} impurity and did not change much in shape with thermal treatments. Another single sharp line, located close to the free electron value g_e=2.0023, appeared after thermal treatments in all cases and can be assigned to carbonaceous radicals formed by pyrolysis of previously adsorbed organic contaminants. These lines are not likely to bear significant information about changes in the Mo species or the zeolite framework and will not be considered further.

Significant amounts of Mo^{5+} species, having in all cases ESR lineshapes corresponding to axial symmetry, appeared after these catalysts were degassed at temperatures $T_D \geq 473$ K. For sample Mo623, outgassed at T_D=473 K, a relatively broad signal A with $g_\perp$=1.932 (peak at g=1.937) and $g_\parallel$=1.876 was observed (Fig. 6a);

it increased substantially for T_D=600 K (Fig. 6b) and became somewhat broadened and reduced upon further heating, with an additional small signal B having a $g_\perp$ feature peaked at g=1.948 appearing for T_D>700 K (Fig. 6c). For sample Mo793, a signal similar to A appeared with small intensity at 473 K (Fig. 6d); it increased for T_D=573 K, having then $g_\perp$=1.935 (peak at g=1.940) and $g_\parallel$=1.89 (signal C, Fig. 6e), and became also broadened for higher T_D, a small additional signal of type B, with perpendicular peak at g=1.951, appearing at T_D=700 K. In addition, a somewhat sharper signal D appeared at T_D=573 K which, although obscured here by the Mn^{+2} sextet, could be better resolved in other cases (see, e.g., Fig. 7) and showed values $g_\perp$=1.981 (peak at g=1.984), $g_\parallel$=1.825.

For both MoT samples, a substantial fraction of these Mo^{5+} signals generated upon outgassing disappeared or became reversibly broadened when excess O_2 was adsorbed at 295 or 77 K; after the excess O_2 was outgassed at 77 K, or if only small amounts of O_2 were adsorbed (no large excess of gaseous O_2 present), O_2^- radicals (g_1=2.0036, g_2=2.0098, g_3=2.0177) could be observed (Fig. 6e), their g values indicating coordination to Mo(VI) ions. If a sample Mo793 previously outgassed at T_D=700 K was heated overnight under O_2 at 523 K and then outgassed at 295 K, signals B and C decreased substantially, while signal D remained nearly unchanged (Fig. 6f).

ESR spectra were also taken for samples Mo623E and Mo793E. In these, no Mn^{+2} sextet appeared, and sharper Mo^{5+} signals could be resolved. After these samples were outgassed at $T_D \geq 473$ K, a new, more intense signal E having $g_\perp$=1.955 (peak at g=1.961), $g_\parallel$=1.893 could be detected together with signal D (Fig. 7a, b), although the relative proportions between them depended somewhat on the precise sequence of outgassing steps. It was also possible to resolve some hyperfine satellite peaks at both extremes of the spectra; computer simulation of these lines yielded the parameters $A_\perp(D)$=54, $A_\parallel(D)$=102, $A_\perp(E)$=44, $A_\parallel(E)$=88 x 10^{-4} cm^{-1}. Outgassing temperature T_D above 600 K caused a decrease in the overall amplitude of the perpendicular features of signal D, while a series of small peaks and shoulders appeared in the same range (Fig. 7c); these were more or less equally spaced at intervals of ca. 11.5 G, as could be better discerned in the second derivative spectrum (see, e.g., Fig. 7d'). These peaks were not affected by O_2 adsorption.

For these ammonia-treated samples, adsorption of excess O_2 at 77 K led only to a small broadening of both signals D and E (recorded at 77 K), which recovered their full intensity and initial width after re-outgassing at 295 K; O_2^- radicals then appeared superimposed on the spectrum, with larger intensity for sample Mo623E than for Mo793E. A treatment in O_2 at 473 K led also to small or no change in these Mo^{5+} signals (Fig. 7d). They were also unchanged by adsorption of propylene at T=295-373 K; on heating under C_3H_6 up to 423 K, signal E decreased, while signal D remained nearly unchanged (Figs. 7e, f). At 423 K this last signal was also little affected by treatments in H_2, while signal E decreased again substantially.

As is most frequent in Mo-containing catalysts, the ESR signals detected correspond to only a small fraction of the overall Mo present. This can be checked by comparison of the double integrals of the spectra with that

of a standard (copper sulfate, in our case). For example, the spectrum in Fig. 7a was found to correspond to 3.5% of the total Mo.

DISCUSSION

The impregnation of NaY zeolite with AHM followed by conventional activation in air at high temperature (ca. 773 K) leads usually to a loss of zeolite crystallinity, which is substantial (~50%) for zeolites with Mo loadings above 7% MoO_3 by weight (9). The combined results of XRD, IR, surface area, and sorption capacity measurements (Fig. 8) show that for the catalyst preparations studied here, the zeolite structure is largely retained when the molybdate-impregnated material is activated at temperatures below 623 K. After activation at higher temperatures a progressive loss of crystallinity is observed. This occurs therefore during the strong dehydration and dehydroxylation of the zeolite, i.e., when molybdate ions can react and become bonded with the zeolite lattice. The appearance of the IR band at 900-920 cm^{-1}, usually attributed to a Mo-O or Mo=O vibration (3, 6, 9), confirms that new interactions between Mo and oxygen ions (possibly belonging to the zeolite framework) are established. On the contrary, as long as sufficient water remains bonded to the zeolite (as may happen under CRD conditions at low or intermediate temperatures), molybdate species do not interact strongly with the zeolite lattice and the structure of the latter is preserved.

The conditions under which the molybdate-impregnated zeolite is activated affect also its crystallinity. As shown by the XRD (Fig. 1) and IR (Fig. 2) results, the conventionally air-calcined sample MoA had lower crystallinity than sample Mo793, prepared at a comparable temperature by the CRD method. The possible reason for the larger crystallinity in this latter case may lie in the very long time in which the sample was kept under controlled water vapor pressure (10 N m^{-2}) while being heated slowly up to 793 K. Under such hydrothermal conditions Mo-containing species can be distributed more slowly and evenly throughout the zeolite. This better dispersion of Mo may lead to a more even distribution of the strains due to the bonding of molybdenum with the zeolite lattice, so that the lattice's structure and regularity result more stable at high activation temperatures.

The redistribution of Mo species with the thermal CRD treatment is evident from the comparison of the surface and bulk Mo/Si ratios given in Table 1 and Fig. 5. The increase observed in the (Mo/Si) ratio when the temperature is increased from 383 to 623 K can be interpreted in terms of the decomposition and subsequent redispersion of the initially poorly dispersed paramolybdate species deposited on the external surface of the zeolite grains during the impregnation process. Further increase in temperature from 623 to 793 K causes a decrease in (Mo/Si) ratio which is not due to loss of Mo from the catalyst (as checked with chemical analysis) and may therefore correspond to a migration of MoO_3 from the external zeolite surface into the lattice cavities. This redistribution process may involve a "vaporization" of MoO_3, favored by a reaction with water vapor according to the equilibrium

$$MoO_3\,(s) + H_2O\,(v) \leftrightarrow MoO_2(OH)_2\,(v) \qquad (2)$$

which can occur under the CRD activation conditions. Although the vapor pressure of $MoO_2(OH)_2$ is relatively low (1.7×10^{-4} N m^{-2} at 600 K and $1.6 \times l0^{-2}$ N m^{-2} at 793 K (24, 25), the fact that the samples remain a long period of time in contact with water vapor and the short distances across which the diffusion processes need to operate (of the same order as the size of the zeolite grains) make possible the establishment of equilibrium (2) and of an efficient Mo redistribution based on a vaporization-readsorption mechanism. This latter process is essentially the classic one used to prepare Mo monolayers on tin oxide (26) and alumina (27) and, more recently, to redisperse MoO_3 on different MoO_3:Al_2O_3 physical mixtures (28). This mechanism is based on the assumption that if a high temperature, e.g. above 600 K, is maintained for a long period, the MoO_3 concentration will tend to become uniform throughout the zeolite surface, except perhaps inside cavities in which steric hindrance effects may be important. Assuming for the $MoO_2(OH)_2$ molecule a size similar to that of MoO_3, i.e., a diameter of ca. 0.5 nm, its entering into the zeolite small cavities (sodalite cages and hexagonal prims) could be controlled by diffusion, taking place at higher temperature, whereupon the molybdenum species would be more dispersed but also distributed in a more heterogeneous collection of sites so that a larger heterogeneity in Mo-zeolite interactions would exist. This is in agreement with the XPS results, which show in the Mo793 sample a loss of the Mo 3d doublet structure and significant increase in the FWHM of its peaks over those of the Mo623 sample, an observation that can be attributed to a higher heterogeneity in Mo environments and interactions in the Mo793 sample. In the case of sample MoA, no such differences (relative to sample Mo623) are detected in the XPS spectrum. For this sample the (Mo/Si) ratio is much lower than for sample Mo693, but higher than for sample Mo793; this behavior could be expected since during the shorter conventional calcination (4 h in air) both redispersion processes (throughout the external surface first, then into the zeolite pores) will be smaller.

Further insight into the localization of the Mo ions in the zeolite can be obtained by comparing the chemical analysis, XPS, and ESR data of the MoT and MoTE samples. Table 1 shows that for sample Mo623 the surface and bulk Mo/Si ratios were decreased substantially (88 and 90%, respectively) by leaching with ammonia, while this same treatment caused in the Mo793 sample smaller decreases in those values (37 and 58%, respectively). These differences between Mo623 and Mo793 samples reflect overall differences in Mo accessibility and dispersion, perhaps also in the interaction between the Mo species and the zeolite lattice. In other words, the higher percentage of molybdenum extracted in the Mo623 sample indicates that the Mo in it is located mostly on the external surface and in the accessible cavities of the zeolite, while for the Mo793 sample more of the Mo is in the less accessible and more internal cavities of the lattice.

This location of a molybdenum fraction inside the zeolite, and more precisely in the smaller cavities, is supported by the ESR spectra. In these, signals A-C, which constitute the majority of the Mo(V) ions detected in outgassed MoT samples, have characteristics roughly similar to those of reduced Mo centers found on MoO_3 (supported or not) or on related solids (29, 30) after activation in vacuo, in H_2, or in hydrocarbons. One must recall here that since ESR-undetectable reduced Mo centers are also possible, the Mo(V) centers thus observed may represent only a fraction of the total Mo content; in fact, such reduced Mo species not seen by

ESR, interpretable as Mo(IV) or as highly symmetrical Mo(V) ions, are probably the main agents responsible for the generation of O_2^-, upon contact with O_2 at room temperature or below (29). However, from the differences in the Mo(V) ions observed some valid clues can be obtained about the overall behavior of the Mo species in these catalysts. Thus, for the MoT samples examined, ESR spectra showing a superposition of several Mo(V) species are found for higher temperatures of CRD preparation or in situ outgassing. This can be correlated with the Mo 3d XP spectra, in which the lines were broader and less resolved for sample Mo793 than for sample Mo623, indicating a more heterogeneous environment, as said above.

The relatively ill-resolved shapes of signals A-C contrast with the rather better resolved signals D and E, which are the main ones observed in the MoTE samples and must be ascribed also to Mo(V) ions because of their g and hyperfine coupling values. Of these, signal E has also ESR parameters more or less comparable to those of the Mo(V) ions more commonly found in oxides, but the g values of signal D are less usual, and in particular the "anisotropy parameter" $\alpha=g_{\|}/4g_{\perp}=2.1$ found in this case is rather larger than the values usually measured; however, such high α values for Mo(V) have been found by Howe et al. (31) upon decomposition of $Mo(CO)_6$ adsorbed in Y zeolite. Although the interpretation of this fact is not straightforward, it reflects probably an unusual coordination of the Mo(V) ion, possibly as a highly distorted tetrahedron. In any case, the substantially smaller linewidths of signals D and E suggest for the corresponding ions a well-defined coordination geometry, in a situation different from that existing in the partially reduced, more or less dispersed MoO_3 particles or agglomerates present in catalysts prepared by the conventional impregnation procedures and which have not undergone treatment with ammonia solution.

Considering the moderately high pH of the extracting solution, we can postulate that both signals D and E arise from isolated Mo centers remaining in the zeolite after the basic solution depolymerizes the $(MoO_3)_n$ type species formed during calcination. On the other hand, these two ESR signals are much less sensitive to broadening by O_2 at 77 K than the species A-C found in MoT samples; they are also less affected by reduction with H_2 and remain unchanged after adsorption of C_3H_6 at 373 K, in marked contrast to the behavior of Mo(V) ions on conventional supports (29). All these facts indicate that these Mo(V) species are located in the small cavities of the zeolite (sodalite cages or hexagonal prisms). The alternative possibility that these signals could arise from Mo(V) ions made inaccessible to gases by being buried in collapsed sections of the zeolite can be ruled out, since they are easily formed at 473 K after the extraction treatment even for the sample prepared at 623 K. ESR signals A and B (and perhaps also signal C), on the other hand, may correspond to Mo(V) ions at the external zeolite surface, since they are found in sample Mo623, in which no Mo penetration has taken place, according to the XPS data.

The apparent transformation of signal D into a multipeaked signal for high outgassing temperature in MoTE samples is more difficult to explain. A first possibility is that such a structure is due to coupling with neighboring Al ion(s). Whether or not these belong to the zeolite framework is not determinable from the present experimental data; in any case, the number and relative intensities of these lines indicate that two such ions would be interacting with each Mo(V), so that one should not ascribe it to the SI site (inside the

hexagonal prism), since the Si/Al ratio of our zeolite means that at least three Al ions must surround each SI site. Another possibility is that these peaks were due to a superhyperfine coupling of the unpaired electron in a Mo(V) ion with several nitrogen nuclei in the neighborhood, arising from residual NH_3 or NH_4^+ present in the zeolite pores after the extraction step. And this would mean that species D is not in the hexagonal prism but in the sodalite cage. Species E, which shows somewhat greater reactivity toward H_2 or C_3H_6 but whose ESR peak is not broadened by O_2, must be also in the sodalite cage. Positions I' and II' can be thus proposed for these D and E signals; this subject will be discussed in more detail elsewhere. The generation of these species indicates, in any case, that Mo species have diffused into the inner pores of the zeolite structure. The fact that species D can be observed in the Mo793 sample (and not in the Mo623) supports the idea proposed above that during the CRD treatments above 700 K, isolated Mo-containing species are generated (e.g., via reaction 2) and diffuse into the zeolite structure. The much higher amounts of signals D and E found for the extracted samples may mean that only monomeric, tetrahedrally coordinated Mo species (which will be dominant after the alkaline treatment) are able to diffuse efficiently across the framework openings connecting the sodalite cages and the large cavities. Diffusion of such species across the 12-membered rings should be much easier; however, (Mo/Si) ratios measured by XPS show that high temperatures (above ca. 720 K) are also needed to allow substantial penetration of Mo inside the zeolite grains. Probably, the bonding of $MoO_2(OH)_2$-type species to the aluminosilicate structure is stronger than to MoO_3, so that after molybdenum has been efficiently dispersed (at 713 K) on the zeolite external surface, higher temperatures are needed to detach from the latter the species which allow further diffusion of Mo into the bulk of the solid and into the zeolite small cavities. Molybdenum would be there inaccessible to sulfur-containing molecules such as thiophene; part of the loss of HDS activity found in the MoT series upon increasing the T values (13) might be thus explained.

REFERENCES

1. Ward, M. B., and Lunsford, J. H., in "Proceedings of 6th International Zeolite Conference, 1983" (D. H. Olson and A. Bisio, Eds.), Butterworths, 1984.
2. Moorehead, E. L., U.S. Patent 4,297,243 (1981).
3. Dai, P. E., and Lunsford, J. H., J. Catal. 64, 173 (1980).
4. Johns, J. R., and Howe, R. F., Zeolites 5, 251 (1985).
5. Abdo, S., and Howe, R. F., .J. Phys. Chem. 87, 1713 (1483).
6. Gallezot, P., Coudurier, G., Primet, M., and lmelik, B., ACS Symp. Ser. 40, 144 (1977).
7. Chen. L. Y., and Hsu, T. C., J. Chin. Inst. Chem. Eng. 2, 25 (1971).
8. Kovacheva, P., Davidova, N., and Shopov, D., Zeolites 3, 92 (1983).
9. Cid, R., Gil Llambias, F. J., Fierro, J. L. G., López Agudo, A., and Villaseñor, J., .J. Catal. 89, 478 (1984).
10. Vysotskii, A. V., Chuikova, N. A., and Lipovich, V. G., Kinet Katal. 18, 1345 (1977).
Il. Balakrishnan, I., Hedge, S. G., Rao, B. S., Kulkami, S. B., and Ratnasamy, P., in "Proceedings of Climax 4th International Conference on the Chemistry and Uses of Molybdenum, 1982" (H. F. Barry and P. C. H. Mitchell, Eds.), p. 331. Climax Molybdenum, Ann Arbor, MI, 1982.

12. Wilhelm, F. C., Tsigdinos, G. A., and Ference, R. A., in 'Proceedings of Climax 3rd Intemational Conference on the Chemistry and Uses of Molybdenum, 1979" (H. F. Barry and P. C. H. Mitchell, Eds.), p. 219. Climax Molybdenum, Ann Arbor, MI, 1979.

13. López Agudo, A., Cid, R., Orellana, F., and Fierro, J. L. G., Polyhedron 5, 187 (1986).

14. Swanson, W. W., Strensand, B. J., and Tsigdinos, G. A., in "Proceedings of Climax 4th Intemational Conference on the Chemistry and Uses of Molybdenum, 1982" (H. F. Barry and P. C. H. Mitchell, Eds.), p. 323. Climax Molybdenum, Ann Arbor, MI, 1982

15. Cid, R., Villaseñor, J., Fierro, J. L. G., and López Agudo, A., Appl. Catal. 18, 357 (1985).

16. Davidova, N., Kovacheva, P., and Shopov, D., Zeolites 6, 304 (1986).

17. Fierro, J. L. G., Rojo, J. M., and Sanz, Colloids Surf. 15, 75 (1985).

18. Flanigen, E. M., and Khatami, H., Adv. Chem. Ser. 101, 201 (1971).

19. Scherzer, J., and Bass, J. L., J. Catal. 28, 101 (1973).

20. Okamoto, T., Nakano, H., and Shimokawa, T., J. Catal. 50, 447 (1977).

21. Patterson, T., Carver, J., Leyden, D., and Hercules, D., J. Phys. Chem. 80, 1700 (1976).

22. Gajardo, P., Grange, P., and Delmon, B., J. Catal. 63, 201 (1980).

23. Wagner, C. D., Davis, L. E., Zeller, M. V., Taylor, J. A., Raymod, R. H., and Gale, L. H., Surf. Interface Anal. 3, 211 (1981).

24. Glemser, O., and Haeseler, R. V., Z. Anorg. Allg. Chem. 316, 168 (1962).

25. Nicolau, I., Aguilo, A., and de Groot, P. B., in "Proceedings of Climax 4th International Conference on the Chemistry and Uses of Molybdenum, 1982" (F. Barry and P. C. H. Mitchell, Eds.), p. 234. Climax Molybdenum, Ann Arbor, MI, 1982.

26. Buiten, J., J. Catal. 10, 188 (1968).

27. Sonnemans, J., and Mars, P., J. Catal. 31, 209 (1973).

28. Leyrer, J., Zaki, M. I., and Knözinger, H., J. Phys. Chem. 90, 4775 (1986).

29. Zhan, R. Y., Narayana, M., and Kevan, L., J. Chem, Soc. Faraday Trans I 81, 2083 (1985).

30. Che, M., Louis, C., and Tatibouet, Polyhedron 5, 123 (1986); Haber, J., and Serwicka, E., Polyhedron 5, 107 (1986).

31. Rommelfaenger, P., and Howe, R. F., J. Chem. Soc. Chem. Commun., 123 (1979); Abdo, S., and Howe, R. F., J. Phys. Chem. 87, 1722 (1983).

TABLE 1

Surface Composition (XPS)[a] and Chemical Analysis of Samples

Sample	$(Mo/Si)_s$	$Mo/(Si + Al)_s$	$(Mo/Si)_{chem}$	$Mo/(Si + Al)_{chem}$
NaY	0.000	0.000	0.000	0.000
Mo 283	0.089	0.061	—	—
Mo 623	0.329	0.220	0.111	0.077
Mo 713	0.077	0.056	—	—
Mo 793	0.041	0.031	0.100	0.070
Mo 623E	0.033	0.023	0.011	0.008
Mo 793E	0.026	0.018	0.042	0.030
MoA	0.063	0.045	—	—

[a] Sensitivity factors taken from Ref. (*23*).

Captions of Figures

Fig. 1. X-ray powder diffraction patterns for NaY, Mo383, Mo623, Mo713, Mo793, and MoA samples.

Fig. 2. Framework infrared spectra in the mid-wavenumber region for (a) NaY, (b) Mo383, (c) Mo623, (d) Mo713, (e) Mo793, and (f) MoA.

Fig. 3. Extent of the water (O) and n-hexane (□) adsorptions at 297 K on the Mo793 sample. Filled symbols refer to the blank NaY zeolite.

Fig. 4. Detailed XP spectra for molybdenum on different Mo-loaded NaY preparations: (a) Mo383, (b) Mo623, (c) Mo713, (d) Mo793, (e) Mo623E, (f) Mo793E, and (g) MoA

Fig. 5. Effect of the calcination temperature and procedure on the Mo/Si ratios of the samples as given by chemical analysis (□) and by XPS: (O), MoT series, (●) MoTE series, and (◊), MoA sample. Bars indicate estimated error.

Fig. 6. ESR spectra of MoT samples. For sample Mo623 (measured at 295 K): (a) outgassed 0.5 h at 373 K, then 1 h at 473 K; (b) after further outgassing (1 h) at 603 K; (c) after further outgassing (1 h) at 793 K. For sample Mo793 (measured at 77 K): (d) outgassed 1 h at 373 K and 1 h at 473 K; (e) subsequently outgassed 1 h at 573 K; (f) heated overnight under O_2 at 523 K, then outgassed at 295 K. Sharp peaks marked with asterisk are due to Mn^{2+} impurity. The dashed line in spectra e and f marks the $g_{\perp}$ peak of signal D, overlapping one of the Mn^{2+} lines.

Fig. 7. ESR spectra of MoTE samples. (a) Sample Mo623, outgassed 1 h at 573 K (measured at 295 K). For sample Mo793E: (b) outgassed 2 h at 473 K; (c) subsequently outgassed (1 h) at 723 K; (d) heated 3 h under O_2 at 473 K (d', second derivative spectrum); (e) new sample portion outgassed 2 h at 393 K, then 1 h at 573 K; (f) subsequently heated under 3.7 kN m^{-2} propylene (1 h) at 423 K. Spectra b-d measured at 77 K, spectra e-f measured at 295 K. Peaks marked with asterisk are due to hyperfine satellites arising from isotopes ^{95}Mo and ^{97}Mo (25% natural abundance).

Fig. 8. Variation of crystallinity (O) and specific area (Δ) with respect to the MoO_3:NaY physical mixture, and n-hexane (□) and water ( ) sorption capacities with respect to NaY zeolite, as a function of the calcination temperature of the MoT series.

Fig. 1

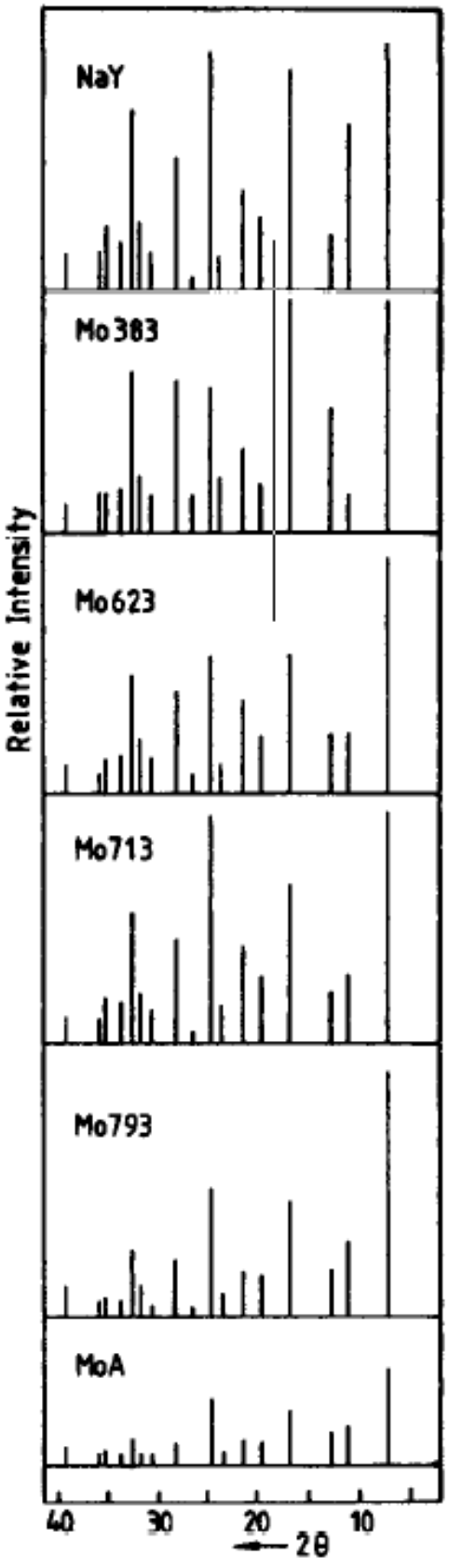
NaY
Mo383
Mo623
Mo713
Mo793
MoA
Relative Intensity
40
30
20
10
2θ

Fig. 2

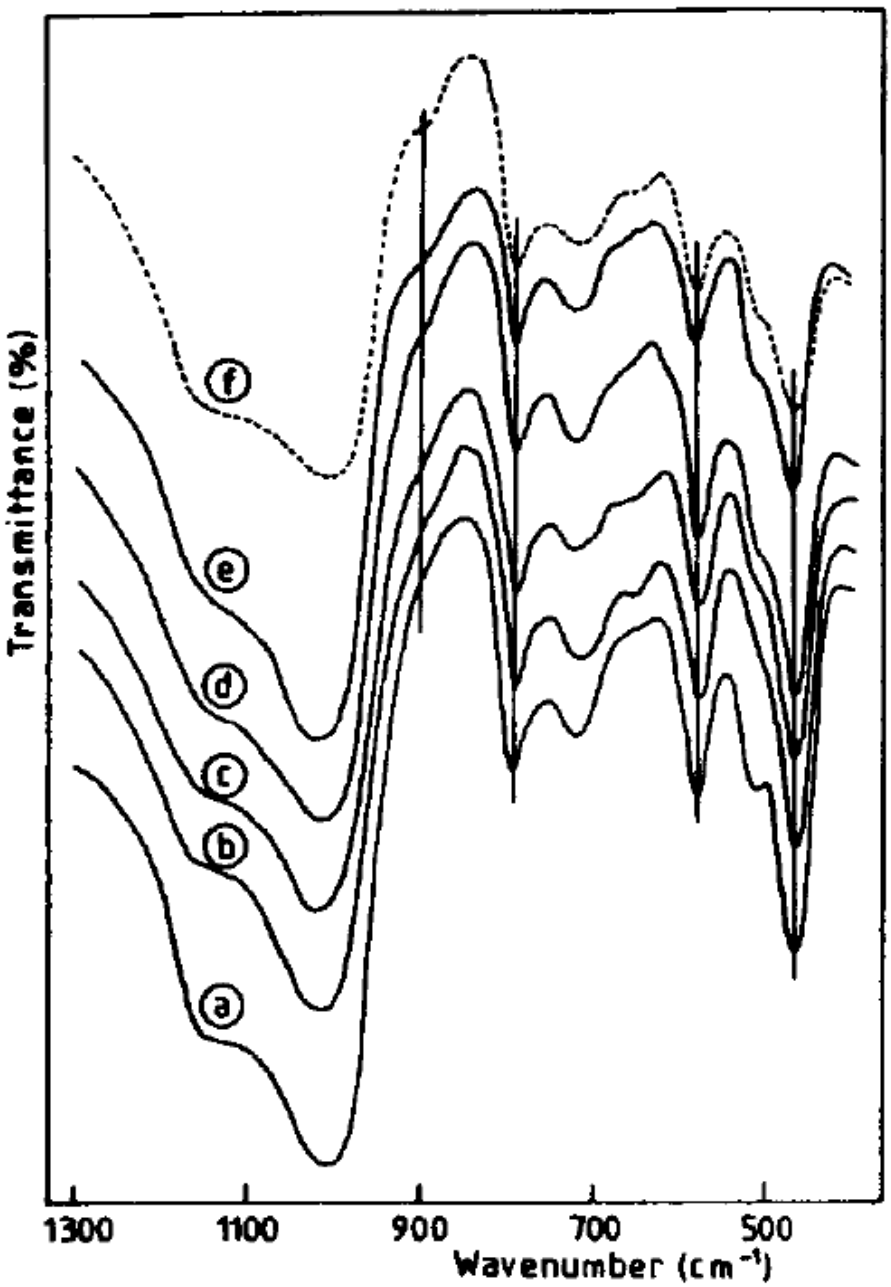

Fig. 3

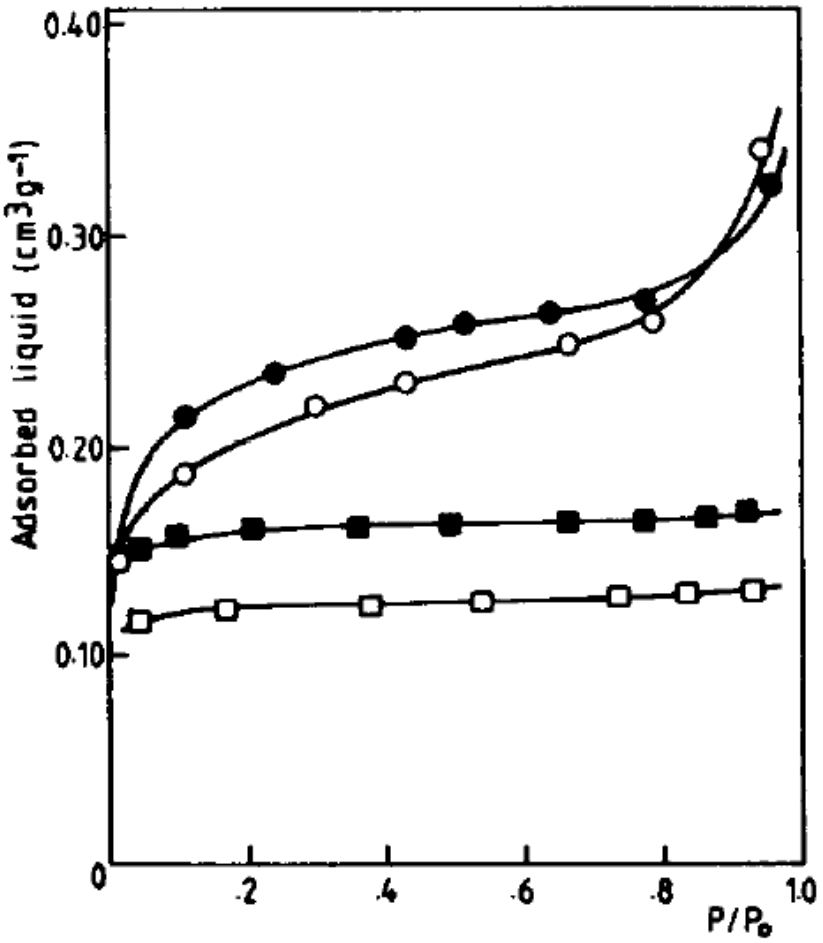

Fig. 4

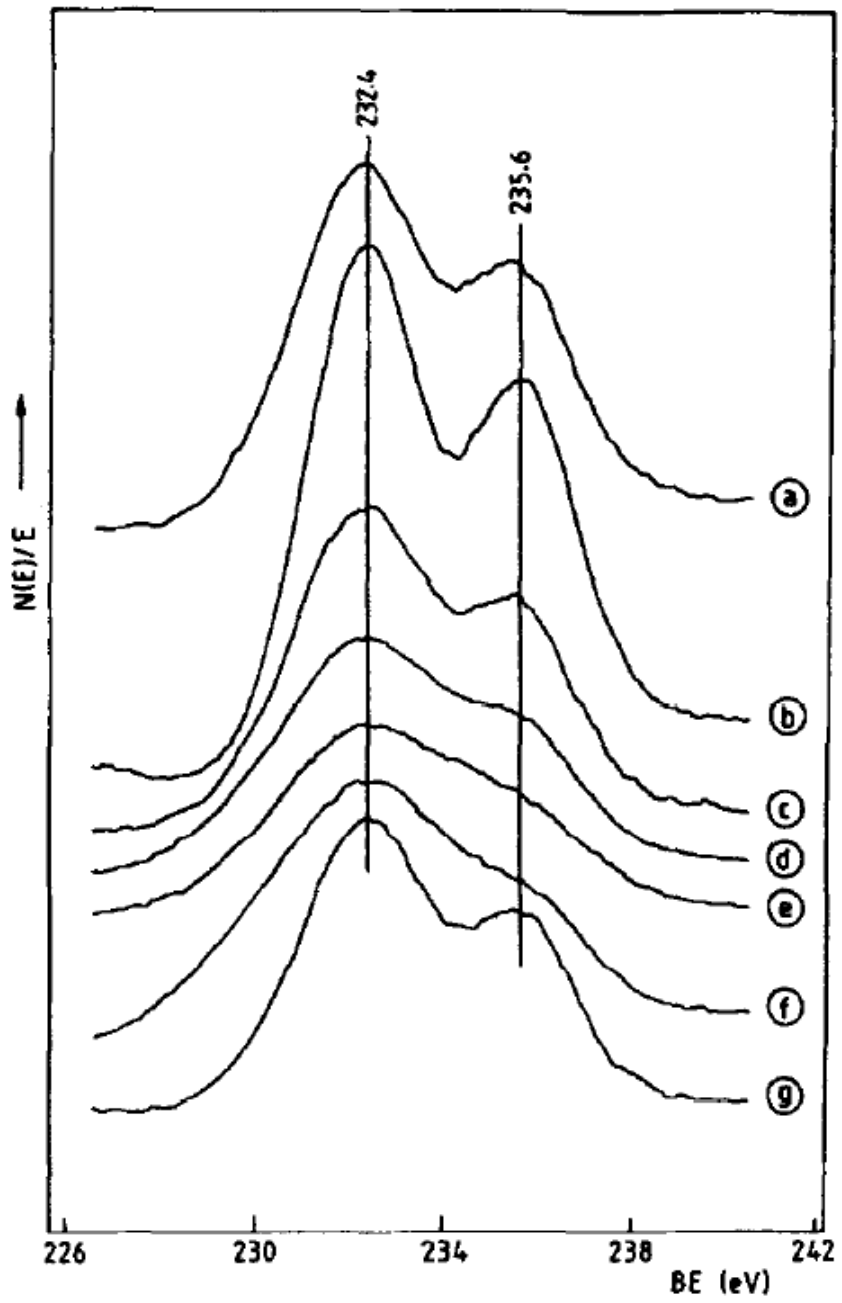

Fig. 5

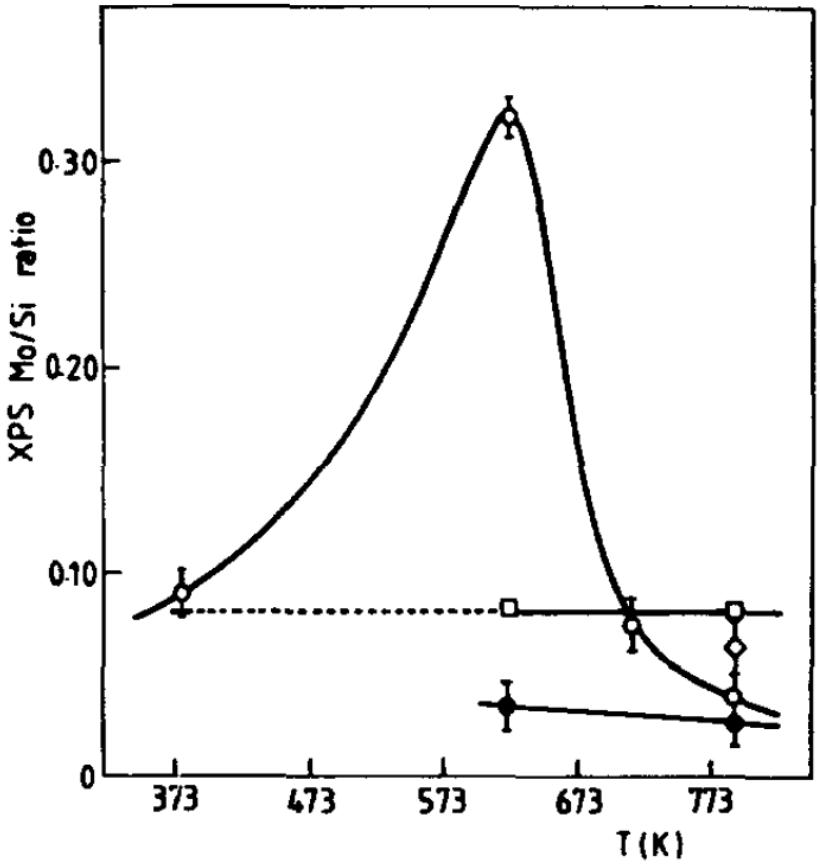

Fig. 6

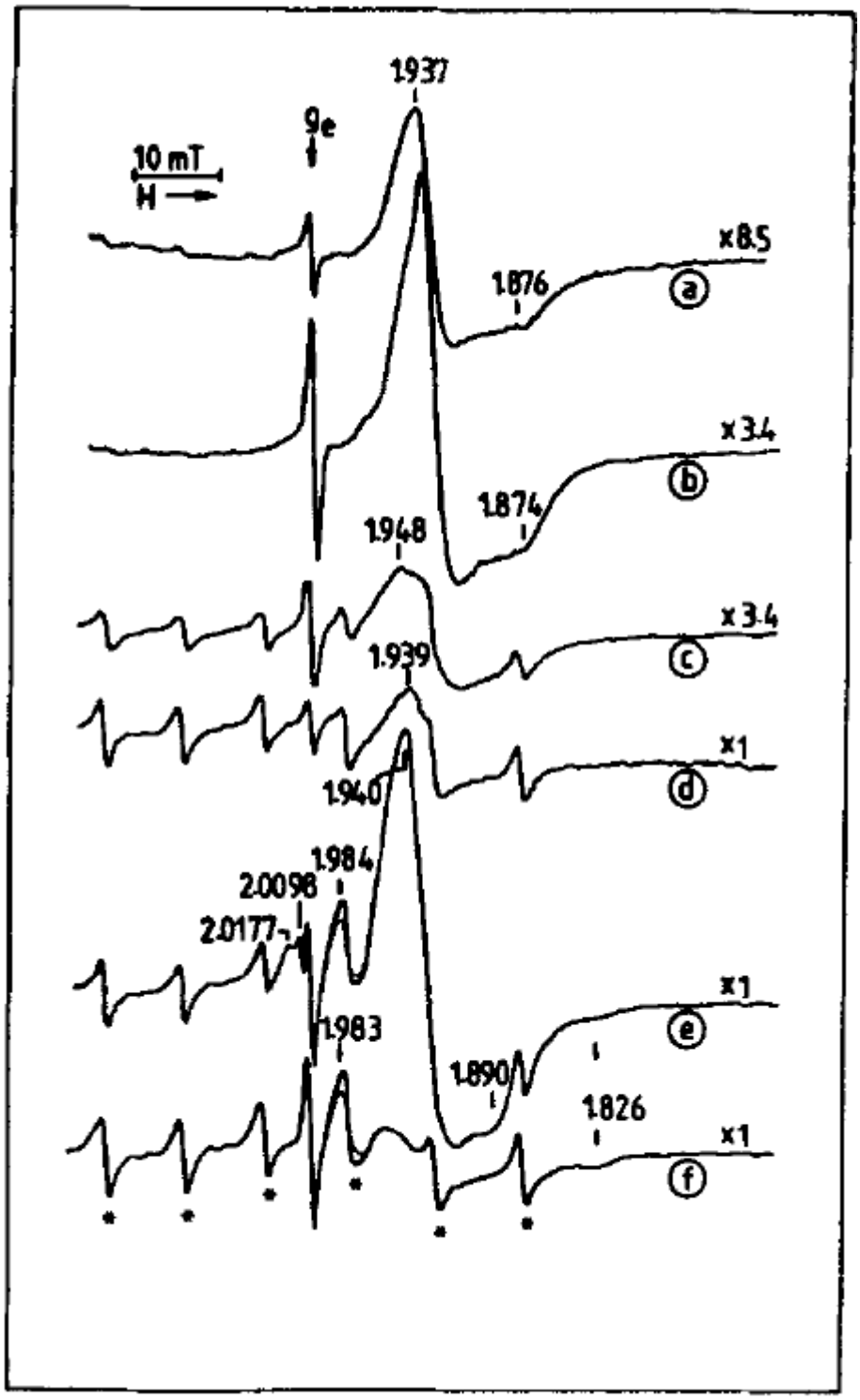
1.937
ge
10 mT
H
x8.5
1.876
a
x3.4
b
1.874
1.948
x3.4
1.939
c
x1
1.940
d
1.984
2.0098
2.0177
x1
1.983
e
1.890
1.826
x1
f

Fig. 7

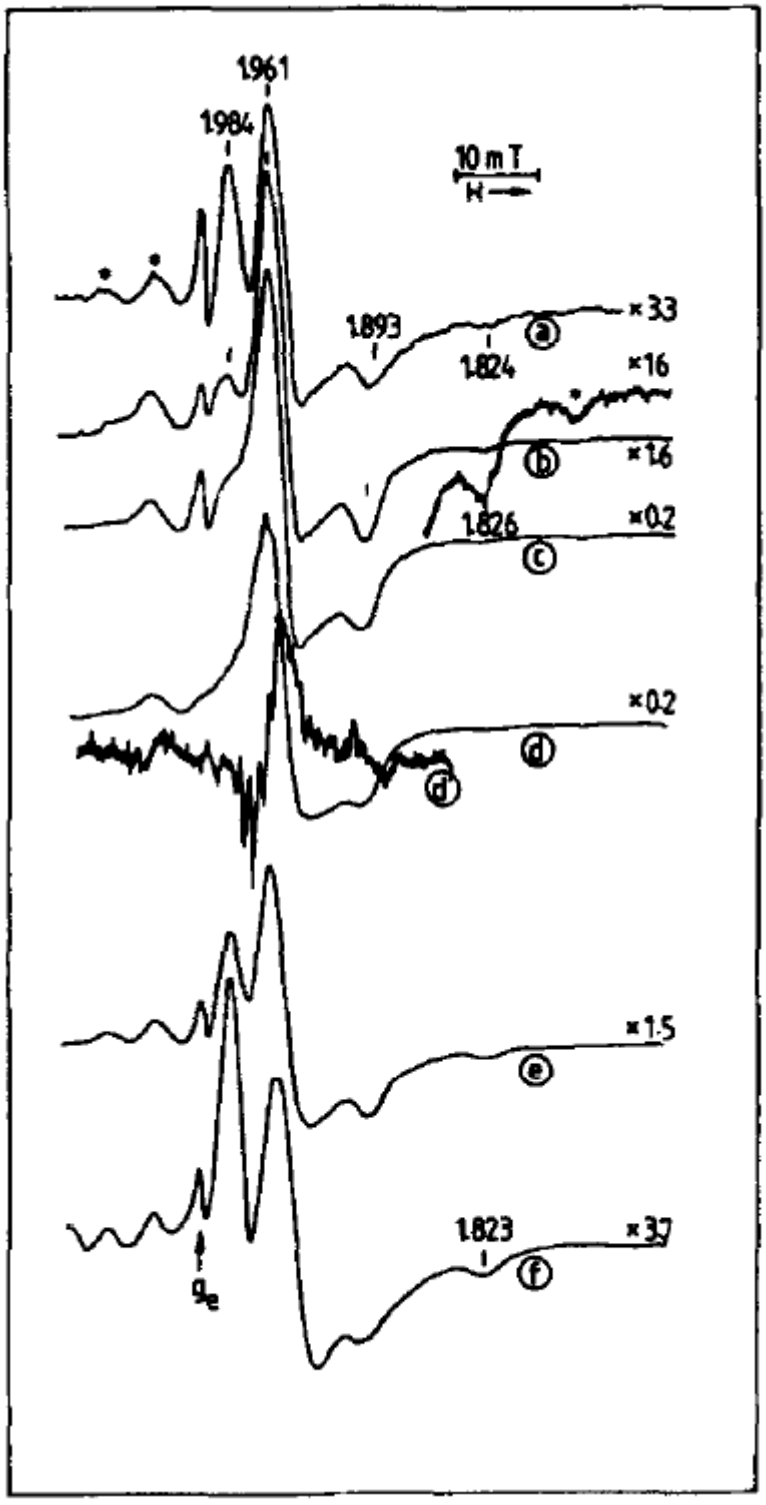
1.961
1.984
10 mT
H
1.893
1.824
×33
a
×16
b
×1.6
1.826
×0.2
c
×0.2
d
d
×1.5
e
1.823
×3.7
f
g_e

Fig. 8